Carbohydrate Polymers 90 (2012) 1016–1023

Contents lists available at SciVerse ScienceDirect

Carbohydrate Polymers

journal homepage: www.elsevier.com/locate/carbpol

Modified coaxial electrospinning for the preparation of high-quality ketoprofen-loaded cellulose acetate nanofibers

Deng-Guang Yu[a,*], Jia-Hui Yu[b], Lan Chen[c], Gareth R. Williams[d], Xia Wang[a,*]

[a] School of Materials Science & Engineering, University of Shanghai for Science and Technology, Shanghai 200093, China
[b] Institutes for Advanced Interdisciplinary Research, East China Normal University, Shanghai 200062, China
[c] School of Medical Instrument and Food Engineering, University of Shanghai for Science and Technology, Shanghai 200093, China
[d] School of Human Sciences, Faculty of Life Sciences, London Metropolitan University, 166-220 Holloway Road, London N7 8DB, UK

ARTICLE INFO

Article history:
Received 12 May 2012
Received in revised form 1 June 2012
Accepted 13 June 2012
Available online 21 June 2012

Keywords:
Coaxial electrospinning
Cellulose acetate
Nanofibers
Sheath fluids
Sustained drug release

ABSTRACT

This study investigates the use of a modified coaxial electrospinning process in the production of drug-loaded cellulose acetate (CA) nanofibers. With CA employed as a filament-forming matrix and ketoprofen (KET) as an active pharmaceutical ingredient, modified coaxial processes using sheath fluids comprising only mixed solvents were undertaken. With a sheath-to-core flow rate ratio of 0.2:1, the nanofibers prepared from the coaxial process had a smaller average diameter, narrower size distribution, more uniform structures, and smoother surface morphologies than those generated from single fluid electrospinning. In addition, the coaxial fibers provided a better zero-order drug release profile. The use of a sheath solvent means that the core jet is subjected to electrical drawing for a longer period, facilitating homogeneous core jet solidification and retarding the formation of wrinkles on the surface of the nanofibers. This modified coaxial electrospinning protocol allows the systematic fabrication of functional polymer nanofibers with improved quality.

© 2012 Elsevier Ltd. All rights reserved.

1. Introduction

Cellulose, the primary structural component of the cell walls of green plants and the most abundant natural resource on earth, is a linear polysaccharide which has many advantageous properties including biocompatibility, biodegradability, and regenerative properties (Deng et al., 2010; Qi, Sui, Yuan, Wei, & Zhang, 2010). Cellulose acetate (CA), the acetate ester of cellulose, has been widely investigated for a wide variety of potential applications in the form of electrospun nanofiber mats. Such applications include as affinity membranes (Ma, Kotaki, & Ramakrishna, 2005), antimicrobial membranes (Abou-Zeid et al., 2011; Anitha, Brabu, Thiruvadigal, Gopalakrishnan, & Natarajan, 2012), three-dimensional structures resembling the urinary bladder matrix (Han & Gouma, 2006), filament-forming matrices for biomedical nanocomposites (Wongsasulak, Patapeejumruswong, Weiss, Supaphol, & Yoovidhya, 2010), and as biosensor strips (Khatri, Wei, Kim, & Kim, 2012). CA fiber mats have additionally been studied for water treatment (Tian et al., 2011) and biomedical separation (Tsioptsias, Sakellariou, Tsivintzelis, Papadopoulou, & Panayiotou, 2010). In particular, CA-based drug-loaded nanofibers are attracting increasing attention for topical and transdermal delivery systems (Taepaiboon, Rungsardthong, & Supaphol, 2007; Wu, Branford-White, Zhu, Chatterton, & Yu, 2010).

Since it has good electrospinnability, CA-based functional nanomaterials are often generated directly using single fluid electrospinning. This is a popular procedure for producing nanofibers due to its ease of implementation and cost-effectiveness (Deng et al., 2011; Yu et al., 2009). Although electrospinning is simple and straightforward to undertake, the mechanism of fiber formation involves complex electro-fluid-mechanical issues and there are many factors that can affect fiber diameters and morphology. Controlled production of polymer nanofibers with uniform diameter and structure remains a challenge (Greiner & Wendorff, 2007; Huang, Zhang, Kotaki, & Ramakrishna, 2003). To ensure successful electrospinning, the chain-entanglement density in the working solution must be high enough to prevent capillary breakup and to subdue Rayleigh instability. This requires a relatively high polymer concentration. However, high concentration polymer solutions often result in clogging of the spinneret and failure of the electrospinning process. Thus, electrospinnable polymer solutions often have narrow concentration windows, and the objective of

* Corresponding authors at: School of Materials Science & Engineering, University of Shanghai for Science and Technology, 516 Jungong Road, Yangpu District, Shanghai 200093, China. Tel.: +86 21 55271687; fax: +86 21 55270632.
E-mail addresses: ydg017@usst.edu.cn (D.-G. Yu), wangxia@usst.edu.cn (X. Wang).

0144-8617/$ – see front matter © 2012 Elsevier Ltd. All rights reserved.
http://dx.doi.org/10.1016/j.carbpol.2012.06.036

reducing fiber diameter (such as by lowering polymer concentration, adding salt or surfactant, or manipulating the spinning parameters) often requires sacrificing fiber uniformity (Fridrikh, Yu, Brenner, & Rutledge, 2003; Yang & Yu, 2012).

Acetone solutions of CA cannot be easily electrospun owing to fast clogging of the spinnerets, and additionally the resultant materials often comprise "bead-on-string" fibers and microparticles (Tungprapa, Jangchud, & Supaphol, 2007). Clogging is a critical but common problem experienced during electrospinning, especially when a high-volatility solvent is used to prepare a polymer solution (Kanjanapongkul, Wongsasulak, & Yoovidhya, 2010a, 2010b). It is a frequent concern for the electrospinning of CA solutions containing acetone, which has a boiling point of only 56 °C, resulting in clogging of the spinneret and poor nanofiber quality. Thus, in recent years, many types of solvent systems have been investigated to achieve smooth and continuous electrospinning of CA. In these systems, acetone is always the main component, which means that the clogging phenomenon can be ameliorated but not completely eliminated (Ahn et al., 2012; Ma et al., 2005; Son, Youk, Lee, & Park, 2004; Tungprapa, Puangparn, et al., 2007; Wu et al., 2010).

Coaxial electrospinning, in which a concentric spinneret can accommodate two different liquids, is regarded as one of the most significant breakthroughs in electrospinning (Zenis, 2004). It has been applied widely in controlling fiber secondary structures (Yarin, 2011), encapsulating drugs or biological agents into fibers (Zhang et al., 2009), preparing nanofibers from materials that lack filament-forming properties (Yu, Fridrikh, & Rutledge, 2004), and enclosing functional liquids within the fiber matrix (Díaz, Barrero, Márquez, & Loscertales, 2006). It would intuitively be expected that, for successful coaxial electrospinning, the sheath fluids must be electrospinnable and have sufficient viscosity to overcome the interfacial tension between the two solutions through "viscous dragging" and "contact friction" (Ma, Fang, Liu, Zhu, & Nie, 2012; Moghe & Gupta, 2008).

However, we have recently developed a modified coaxial electrospinning process in which only unspinnable organic solvents were deployed as sheath fluids. Such a sheath solvent can stabilize the electrospinning process and assists the generation of high quality nanofibers (in terms of their size distribution, uniformity and surface morphology). The modified processes has resulted in several developments, including manipulating the size of nanoparticles self-assembled from polyvinylpyrrolidone (PVP)-based composite nanofibers (Yu, Zhu, Branford-White, Bligh, & White, 2011), preparing ultrafine fibers from concentrated PVP solutions (Yu et al., 2010), systematically improving PVP fiber quality (Yu, Branford-White, et al., 2011), and obtaining finer polyacrylonitrile fibers as precursors for carbon nanofibers (Yu, Lu, Branford-White, Yang, & Wang, 2012; Yu, Williams, et al., 2012). The modified coaxial process opens a new route to generate nanofibers from polymer solutions through partially replacing the traditional interface between polymer jets and the atmosphere by one between polymer jets and sheath solvents.

Building on the developments discussed above, this study investigates the preparation and properties of drug-loaded CA nanofibers generated using modified coaxial electrospinning. In contrast to literature reports on the electrospinning of CA nanofibers, owing to the sheath solvents there are no problems with clogging of the spinneret, and the resultant nanofiber quality is improved substantially. Expanding on our previous studies of modified coaxial electrospinning, here we demonstrate that nanofibers from the modified coaxial process not only have higher quality, but also exhibit improved functional performance.

2. Experimental

2.1. Materials

Cellulose acetate (CA, white powder; *Mw* = 100 000 Da) was purchased from Acros (NJ, USA), and used as received. Ketoprofen (KET) was purchased from Wuhan Fortuna Chemical Co. Ltd. (Hubei, China). N,N-dimethylacetamide (DMAc), acetone, and anhydrous ethanol were purchased from the Sinopharm Chemical Reagent Co. Ltd. (Shanghai, China). All other chemicals used were analytical grade, and water was doubly distilled immediately before use.

2.2. Modified coaxial electrospinning

The core electrospinnable CA solutions were prepared by dissolving 11 g CA and 2 g KET in 100 mL of a solvent mixture comprising acetone, DMAc, and ethanol in the ratio 4:1:1 by volume. The flow rate for spinning was fixed at 1.0 mL/h. A solvent mixture of acetone, DMAc, and ethanol (4:1:1 by volume) was used as the sheath fluid, and sheath flow rates of 0, 0.2, and 0.4 mL/h were explored. The resulting nanofibers were denoted F1 (0 mL/h sheath flow rate), F2 (0.2 mL/h), and F3 (0.4 mL/h) respectively. In addition, a co-dissolving solution of 5.5 g CA and 1 g KET in 60 mL of the same acetone/DMAc/ethanol solvent mixture was subjected to single fluid electrospinning with a flow rate of 1.2 mL/h (yielding F4) for comparison (Table 1).

Two syringe pumps (KDS100 and KDS200, Cole-Parmer, IL, USA) and a high-voltage power supply (ZGF 60 kV/2 mA, Shanghai Sute Corp., Shanghai, China) were used for electrospinning. Following some optimization, the applied voltage was fixed 15 kV and the fibers collected on aluminum foil at a distance of 15 cm. All electrospinning processes were carried out under ambient conditions (21 ± 3 °C with relative humidity 57 ± 6%). Electrospinning was recorded using a digital video recorder (PowerShot A490, Canon, Tokyo, Japan). A self-made concentric spinneret was used to conduct the coaxial electrospinning process.

2.3. Characterization

The morphology of the nanofiber mats was assessed using an S-4800 field emission scanning electron microscope (FESEM) (Hitachi, Tokyo, Japan). Prior to the examination, the samples were

Table 1
Experimental parameters for the fabrication of KET-loaded CA nanofibers.

No.	Process	C_{CA}[a] (% w/v)	Flow rate (mL/h)		Fiber morphology	Diameter (nm)
			Sheath	Core		
F1	Single	11	0	1.0	Linear	660 ± 150
F2	Coaxial	11	0.2	1.0	Linear	240 ± 30
F3	Coaxial	11	0.4	1.0	Mixed morphologies	–
F4	Single	9.17	0	1.2	Bead-on-string	–

[a] C_{CA} refers to CA concentration in mixed solvent of acetone:DMAc:ethanol (4:1:1 in volume).

gold sputter-coated under an argon atmosphere to render them electrically conductive. Images were then recorded at an excitation voltage of 3 kV. The average fiber diameter was determined by measuring their diameters in FESEM images at more than 100 different points using the ImageJ software (National Institutes of Health, MD, USA). Differential scanning calorimetric analyses (DSC) were carried out using a MDSC 2910 differential scanning calorimeter (TA Instruments Co., DE, USA). Sealed samples were heated at 10 °C min^{-1} from 20 to 250 °C under a nitrogen flow of 40 mL/min. X-ray diffraction patterns (XRD) were obtained on a D/Max-BR diffractometer (RigaKu, Tokyo, Japan) with Cu Kα radiation in the 2θ range 5–60° at 40 mV and 30 mA. Attenuated total reflectance Fourier transform infrared (ATR-FTIR) analysis was performed on a Nicolet-Nexus 670 FTIR spectrometer (Nicolet Instrument Corporation, WI, USA) over the range 500–4000 cm^{-1} at a resolution of 2 cm^{-1}.

In vitro dissolution tests were carried out according to the Chinese Pharmacopoeia (2005 ed.) Method II, a paddle method in which a RCZ-8A dissolution apparatus (Tianjin University Radio Factory, Tianjin, China) was used. 100 mg of fibers F1 and F2 were put into 600 mL physiological saline (PS, 0.9 wt%) at 32 ± 1 °C and the instrument was set to 50 rpm, providing sink conditions in which $C < 0.2C_s$. At predetermined time points, samples of 5.0 mL were withdrawn from the dissolution medium and replaced with fresh medium to maintain a constant volume. After filtration through a 0.22 μm membrane (Millipore, MA, USA) and appropriate dilution with PS, samples were analyzed at 260 nm using a UV–vis spectrophotometer (UV-2102PC, Unico Instrument Co. Ltd., Shanghai, China). The cumulative amount of KET released at each time point was back-calculated from the data obtained against a predetermined calibration curve (Wu et al., 2010). Experiments were carried out in triplicate and results are reported as mean values.

3. Results and discussion

3.1. Modified coaxial electrospinning process

A schematic diagram of the modified coaxial electrospinning process is shown in Fig. 1a. A self-made concentric spinneret was employed (Fig. 1b). Two syringe pumps were used to drive the sheath and core fluids independently. An alligator clip was used to connect the inner stainless steel capillary of the spinnaret to the high voltage power supply (Fig. 1c). Under suitable fabrication parameters (core and sheath flow rates of 1.0 and 0.2 mL/h respectively, applied voltage of 15 kV, and spinnaret to collector distance of 15 cm), a fluid jet trajectory similar to those observed in a single fluid electrospinning was created. This comprised a straight thinning jet emitted from a compound Taylor cone, followed by a bending and whipping instability region with loops of increasing size (Fig. 1d). The coaxial process could be undertaken continuously with no user intervention, while in single fluid electrospinning it was from time to time necessary to remove a semi-solid residue which formed on the spinneret to avoid clogging.

The critical voltage applied to a fluid to initiate Taylor cone formation and the straight thinning jet (V_c) has a close relationship with the diameter of the sheath part of the concentric spinneret (Yeo & Friend, 2006);

$$V_c \sim \sqrt{\frac{\gamma d^2}{\varepsilon R}}$$

where V_c is the critical voltage for a jet emanating from the meniscus tip, d is the electrode separation, ε is the permittivity, γ is the surface tension, and R is the principal curvature of the liquid meniscus. A low diameter spinneret orifice gives a high value of R, and thus only a small V_c is needed to initiate electrospinning. The self-made spinneret used in this work has outside and inner diameters of 1.2 and 0.3 mm respectively (Fig. 1c), facilitating the coaxial electrospinning process. In addition, the inner capillary protrudes slightly from the surface of the outer capillary, which should help to ensure that the sheath solvent fully surrounds the core CA solution.

3.2. Morphologies of the KET-loaded CA nanofibers

FESEM images of the F1 nanofibers obtained with a sheath solvent flow rate of zero (essentially a single fluid electrospinning process) are given in Fig. 2a and b. The fibers had an average diameter of 680 ± 150 nm (Fig. 2c). In addition to displaying a wide distribution of diameters, the fibers have numerous wrinkles on their surface, both along and perpendicular to the axial direction (inset of Fig. 2b). Acetone and ethanol evaporate very easily, which made the electrospinning process very sensitive to small changes in the environment and thus produced nanofibers with a wide range of sizes. It also resulted in a solid "skin" on the fiber surfaces, with some solvent still trapped inside the fiber bodies. After spinning, the solvent contained in the fibers diffused out into the atmosphere, and the resulting barometric pressure distorted the cylindrical fibers and generated wrinkles.

The F2 fibers obtained from modified coaxial electrospinning with a sheath-to-core flow rate ratio of 0.2 had more homogeneous structures, smaller diameters, and narrower diameter distributions of 240 ± 30 nm (Fig. 2d–f). The nanofibers also had very smooth surfaces (see inset of Fig. 2e). These results demonstrate that modified coaxial electrospinning is effective in improving surface morphologies, and reducing the diameters and size distributions of KET-loaded CA nanofibers. When the sheath-to-core flow rate ratio was increased to 0.4, the resultant F3 fibers had mixed morphologies, including not only linear fibers and spindrils, but also clumps. The latter result from the excessive amount of sheath fluid causing "wet" fibers to be deposited on the collector and subsequently agglomerating, and are indicated by the arrows in Fig. 2i.

To investigate the influence of the sheath solvent on the formation of KET-loaded CA nanofibers, a solution containing 9.17% (w/v) of CA and 1.67% KET was subjected to a single fluid electrospinning process (using the concentric spinneret with a core fluid

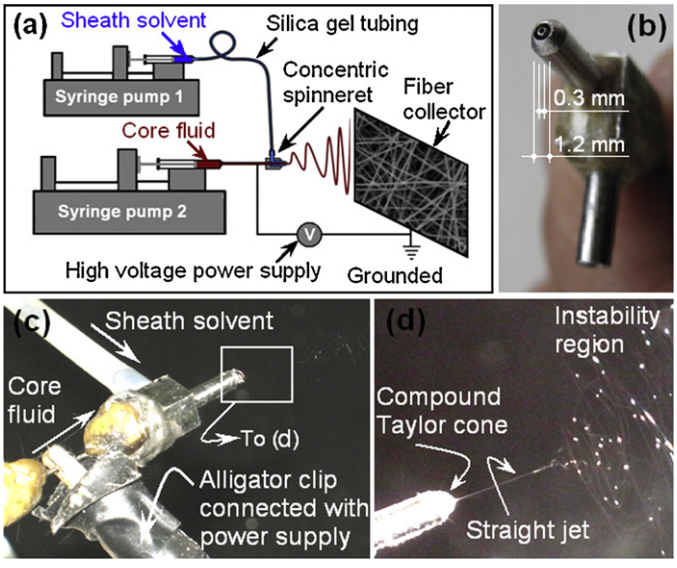

Fig. 1. Modified coaxial electrospinning with solvent as sheath fluid for preparing KET-loaded CA nanofibers: (a) a schematic diagram; (b) the concentric spinneret; (c) the connection between the power supply and the spinneret; (d) a typical fluid jet trajectory (taken under a magnification of 12×) under core and sheath flow rates of 1.0 and 0.2 mL/h respectively, an applied voltage of 15 kV and a fiber collection distance of 15 cm.

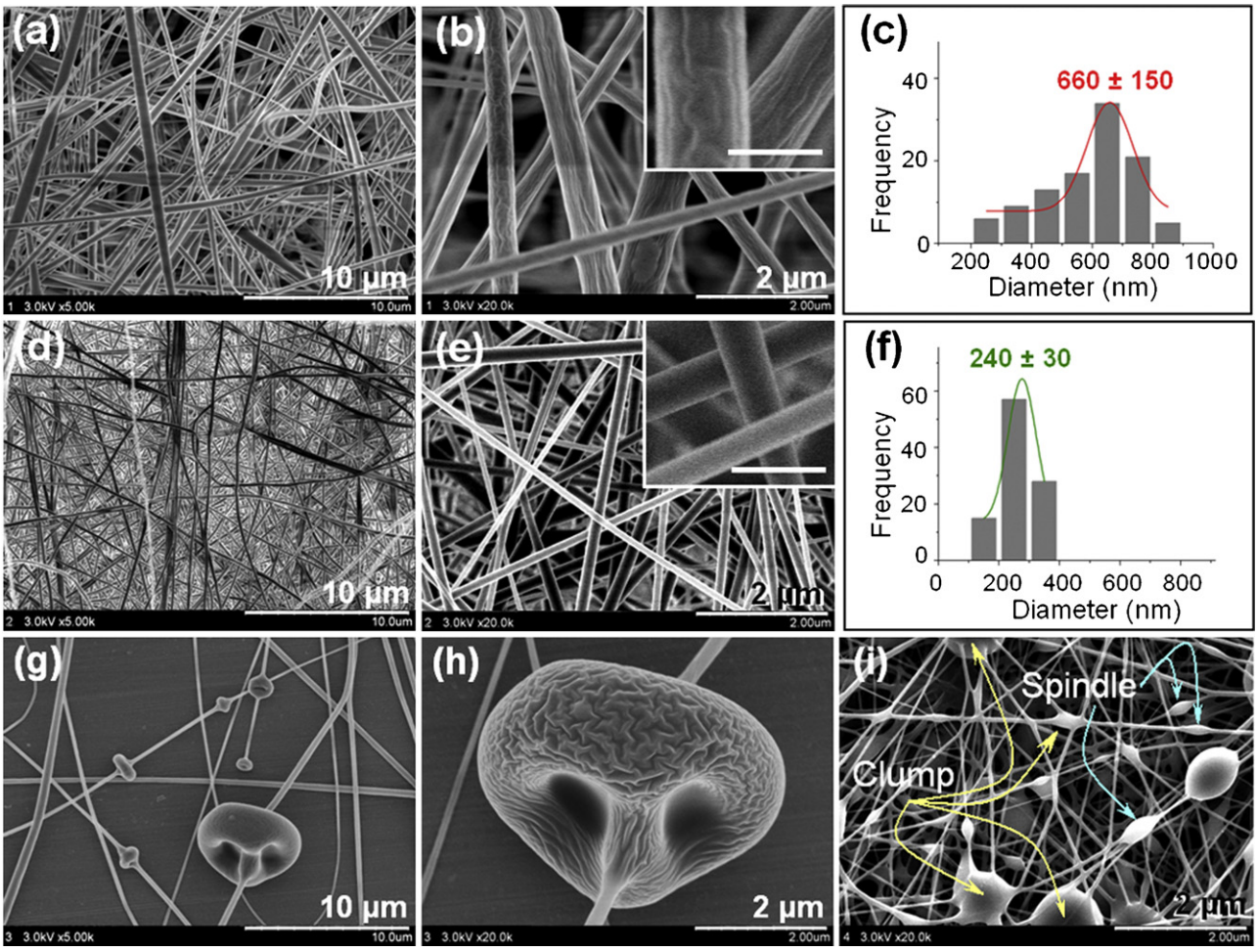

Fig. 2. FESEM images of KET-loaded CA nanofibers prepared using different processes: (a–c) surface morphologies and diameter distribution of F1; (d–f) surface morphologies and diameter distribution of F2 (g and h) surface morphologies of F4; (i) surface morphologies of F3. The scale bars in the insets of (b and e) represent 500 nm.

rate of 1.2 mL/h and a sheath fluid rate of 0 mL/h). This arrangement is analogous to the conditions used to prepare the F2 nanofibers, taking into account the dilution of the core fluid by the sheath fluid. All other electrospinning parameters were kept constant. The F4 nanofibers produced had very distinct beads-on-string morphology due to the spinning solution lacking sufficient polymer entanglements to prevent capillary breakup and Rayleigh instability, required to produce nanofibers with a uniform structure (Fig. 2g and h). Because of the fast evaporation of the solvent at the surface of the fluid jets and the premature formation of a "semi-solid skin," the beads had a flat morphology with many wrinkles on their surfaces (Fig. 2h). Comparing nanofibers F2 and F4, it is clear that the production of high quality KET-loaded CA nanofibers in the coaxial process is not simply a result of dilution of the core solution by the sheath solvent.

3.3. Physical status of KET and its compatibility with matrix CA in the nanofibers

DSC and XRD measurements were undertaken to determine the physical status of KET in the composite nanofibers. DSC thermograms are shown in Fig. 3a. The DSC curve of pure KET exhibited a single endothermic response corresponding to its melting point of 96.24 °C ($\Delta H_f = -114.72$ J/g). Being an amorphous polymer, CA did not show any fusion peaks or phase transitions. DSC thermograms of the medicated fibers F1 and F2 did not show any peaks characteristic of KET melting, suggesting that the drug was no longer present as a crystalline material, but had been converted into an amorphous state.

As depicted in Fig. 3b, the presence of numerous distinct reflections in the XRD pattern of pure KET demonstrated that the pure drug is a crystalline material. The CA diffraction pattern exhibits a diffuse background pattern with one diffraction halo, indicating that the polymer is amorphous. In the patterns of the KET-loaded CA nanofibers F1 and F2 the characteristic reflections of KET were absent, and there was only a hump characteristic of amorphous materials: this demonstrates that KET was no longer present as a crystalline material, but was converted into an amorphous state in the fibers.

The results from DSC and XRD both confirmed that KET was highly distributed in the CA nanofiber matrix, and was present in an amorphous manner where the original structure of the pure materials had been lost. This observation concurred with the observations from FESEM, where no separate particles could be discerned on the surfaces of F1 (Fig. 2a and b) and F2 (Fig. 2d and e).

Compatibility among the components is essential for producing high quality stabile nanofibers. Often second-order interactions such as hydrogen bonding, electrostatic interactions, and hydrophobic interactions improve compatibility. Both KET and CA molecules possess free hydroxyl groups (acting as potential proton donors for hydrogen bonding) and carbonyl groups (potential proton receptors). Therefore it can be speculated that hydrogen bonding interactions can occur within the KET-loaded CA nanofibers.

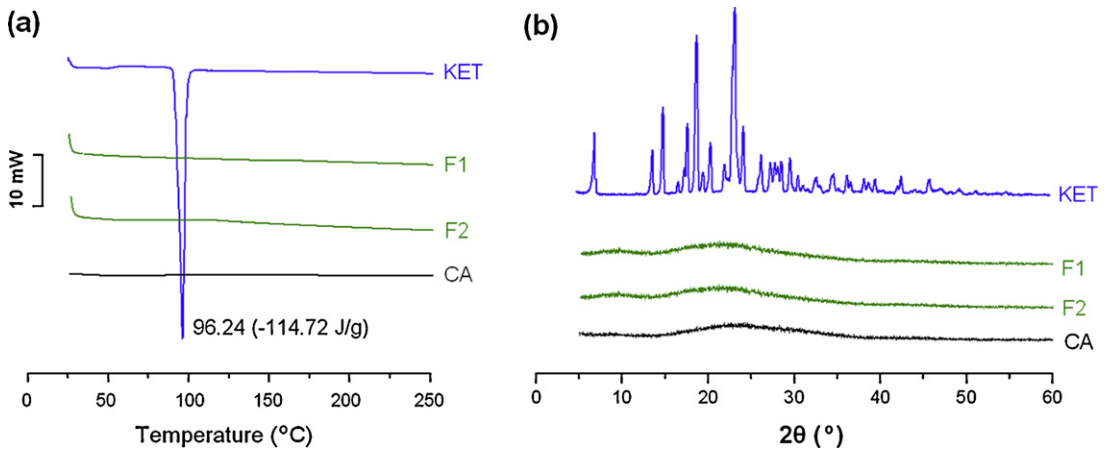

Fig. 3. Physical status characterization: (a) DSC thermograms; and (b) XRD patterns for F1 (prepared by traditional single fluid electrospinning) and F2 (prepared by modified coaxial electrospinning).

FTIR spectra are included in Fig. 4a. Two well-defined, sharp peaks are visible for pure crystalline ketoprofen: one at 1697 cm^{-1}, representing the stretching vibration of the carbonyl group in the KET dimer (see Fig. 4b), and the other at 1655 cm^{-1} due to stretching of the ketone group. The former is observed because KET molecules are bound together in dimers in its crystalline form. However, the peak at 1697 cm^{-1} disappeared in the spectrum of F1 and F2, indicating the breakage of the KET dimers and the formation of hydrogen bonds between the CA carbonyl group and the hydroxyl group of KET (Fig. 4b). KET molecules, by interacting with the polymer, are less likely to form the dimers which are essential for formation of a crystal lattice. Although there may be secondary interactions between KET and CA involving electrostatic and hydrophobic interactions through the KET benzene ring, it is thought to be mainly the KET–CA hydrogen bonding interactions that prevent KET crystallization in the fibers. These interactions stabilize KET in an amorphous state in the nanofibers.

Both single fluid and modified coaxial electrospinning exploit electrical energy to dry and solidify micro-fluid jets. These processes produce nanosize fibers very rapidly, often on the order of 10^{-2} s, causing the physical state of the components in the liquid solutions to be propagated into the solid nanofibers. Thus, nanofibers with KET homogeneously and amorphously distributed on the filament-forming polymer CA can be generated *via* both processes.

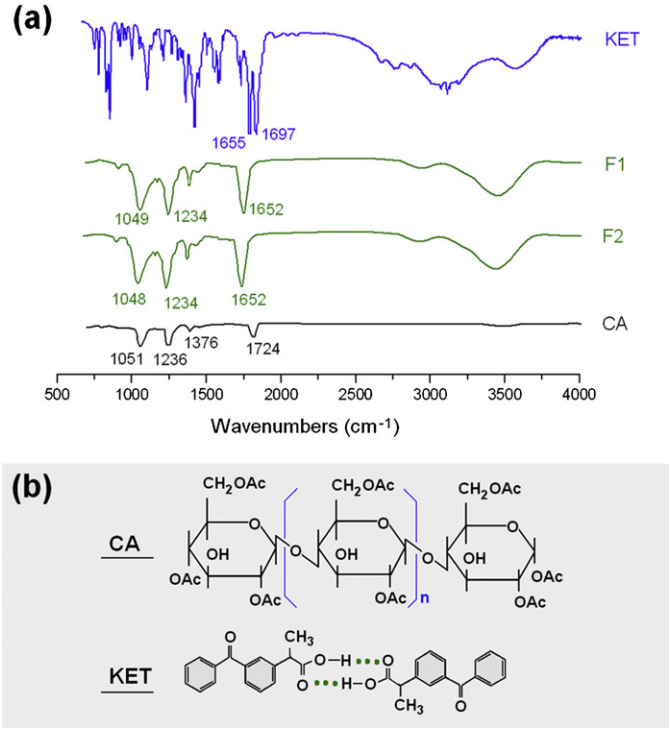

Fig. 4. Compatibility investigation: (a) ATR-FTIR spectra of the components (KET and CA) and fibers F1 (prepared by traditional single fluid electrospinning) and F2 (prepared by modified coaxial electrospinning). (b) Molecular structures of KET and CA, and hydrogen bonding between KET molecules.

3.4. *In vitro* dissolution tests

KET has a UV absorbance peak at 260 nm, and hence the amount of KET released from the fibers was determined by UV spectroscopy using a pre-determined calibration curve $C = 15.27A - 0.0034$ ($R = 0.9996$) where C is the concentration of KET ($\mu g\,mL^{-1}$) and A is the solution absorbance at 260 nm (linear range: 2–20 $\mu g\,mL^{-1}$).

A comparison of the *in vitro* release profiles of KET from fibers F1 and F2 is provided in Fig. 5 and Table 2. Both KET-loaded CA nanofibers provided similar sustained drug release profiles. Sustained release of KET over a period of *ca.* 144 h was observed from both fibers, and similar drug release percentages were recorded after 1 and 8 h (Table 2).

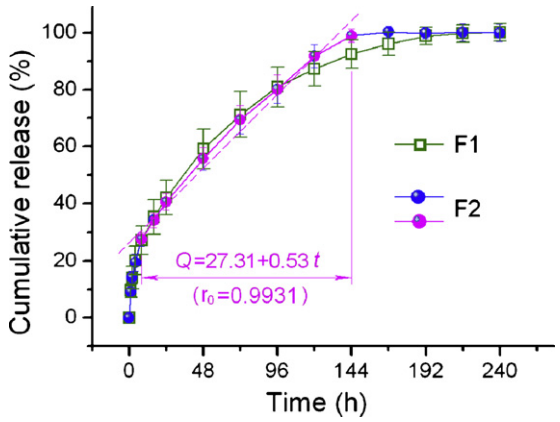

Fig. 5. *In vitro* dissolution profiles of the KET-loaded nanofibers F1 (prepared by traditional single fluid electrospinning) and F2 (prepared by modified coaxial electrospinning).

Table 2
KET release profiles from different CA nanofibers ($n = 6$).

Fiber	R_1 [a] (%)	Linear release parameters				$t_{1/2}$ [b]	Regressed equation	
		Equation	r_0 [c]	R_8 [a] (%)	R_{144} [a] (%)		Peppas equation	r_p [d]
F1	9.5	$Q = 30.23 + 0.48t$	0.9766	27.2	92.4	36	$Q = 10.58t^{0.4318}$	0.9972
F2	9.1	$Q = 27.31 + 0.53t$	0.9931	27.5	98.9	37	$Q = 10.16t^{0.4413}$	0.9964

[a] Percentage of drug after 1, 8, and 144 h.
[b] Time taken to release 50% drug.
[c] Correlation coefficient regressed according to the zero-order release equation from 8 to 144 h.
[d] Correlation coefficient regressed according to the Peppas equation.

The KET release profiles were analyzed according to the Peppas equation (Peppas, 1985):

$$Q = kt^n$$

where Q is the drug release percentage, t is the release time, k is a constant reflecting the structural and geometric characteristics of fibers, and n is the release exponent, which is indicative of the drug release mechanism. The same drug release mechanism was found for both F1 and F2. This is a typical Fickian diffusion mechanism, indicated by a value of the release exponent less than 0.45 (0.4318 for F1 and 0.4413 for F2).

However, there significant differences between the dissolution of the two fibers. First, fiber F2 exhibited a more linear drug release profile than F1, as indicated by a higher correlation coefficient (regressed according to the zero-order release equation from 8 to 144 h; 0.9931 and 0.9766 respectively). Second, the amount of KET unreleased after 144 h is smaller for F2 than F1: 1.1% for the former, and 7.6% for the latter. For zero-order drug release profiles, the smaller the amount of unreleased drug and the shorter the "tailing off" time period the better – this is because drug release in the latter period cannot deliver an effective therapeutic concentration in the blood (Kim, 1995). Thus it can be concluded that the fibers from the modified coaxial electrospinning process (F2) were able to provide a better sustained release profile than those from a single fluid process (F1). This can be attributed to the higher quality of the F2 nanofibers, which have smaller diameters, smoother surfaces, and a narrower distribution of fiber diameters. In contrast, the F1 nanofibers have bigger diameters, wrinkled surface morphologies and a broader distribution of fiber diameters. A larger diameter means a longer distance which the embedded drug must travel if it is to diffuse into the dissolution medium. Combined with the non-uniform distribution of fiber diameters, it is inevitable that the F1 nanofibers will have a longer undesired "tailing off" time. In addition, the larger diameter and wrinkled morphology of F1 aggravate the initial burst release effect, due to an increased surface area available for drug release.

3.5. Mechanism of fiber improvement through the coaxial electrospinning process

Throughout modified coaxial electrospinning, the sheath solvent will: (1) facilitate the formation of the Taylor cone due to lower surface tension of the core fluid; (2) surround the straight thinning jet of the core polymer solution, retarding evaporation of solvent from the core fluid while the sheath solvent itself evaporates to the atmosphere; (3) follow the core fluid when entering the instability region. In the instability regions, where most of the solvents evaporate, the sheath solvent can retard the premature evaporation of core jet solvents, and hence keep the jet in a fluid state for longer. This in turn would keep the inner viscoelastic force of the core KET–CA co-dissolving solutions relatively low (f_4), thus letting electrostatic force (f_1 and f_3) and repulsive forces between the two unstable bending coils (f_2) play an effective role in producing narrower nanofibers such as F2 (Fig. 6a and b). Often, the gravitational force acting on the fluid jets can be ignored, as it is negligible in its influence when compared to other parameters.

The single fluid electrospinning process is very sensitive to environmental changes, in particular when working with volatile

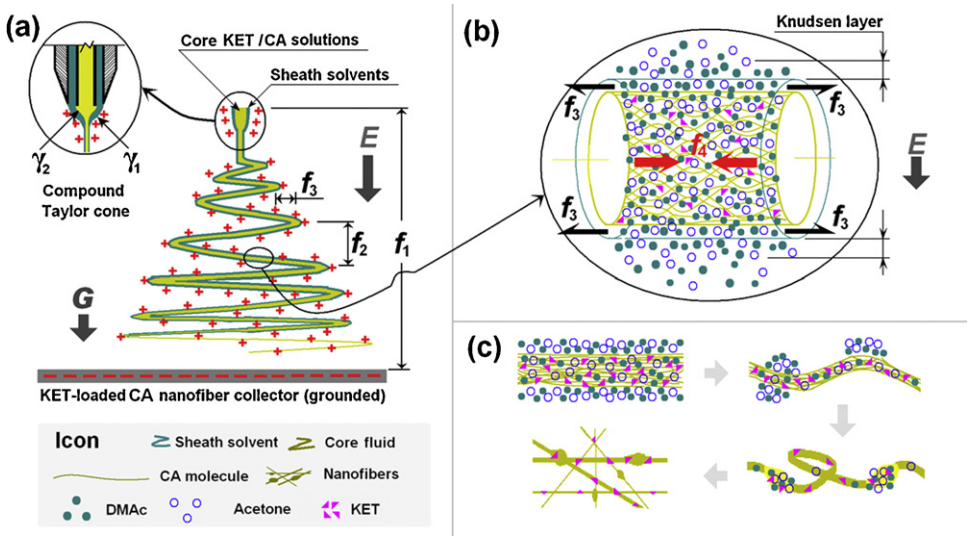

Fig. 6. A schematic diagram demonstrating the effect of sheath solvents on the formation of KET-loaded CA nanofibers: (a and b) the modified coaxial process with a suitable sheath-to-core flow rate ratio; (c) the same coaxial process with an excessive rate of sheath solvent flow. Forces f_1 and f_2 signify the attractive force between the two electrodes and the repulsion forces between two unstable bending coils. f_3 represents the Coulomb repulsion force. f_4 is the counterforce of the fluid jets. G represents the gravitational force. E represents the electrical field. γ_1 and γ_2 represent surface tensions.

organic solvents. The modified process discussed in this paper provided a stable and robust core–sheath interface for the core CA/KET solution when it was drawn in the electrical field (Fig. 6a and b). This protects the core from the disturbance of environmental changes. During their evaporation, the sheath solvents render a stable Knudsen layer permitting gradual and smooth mass transfer of the solvents from the core fluid jets to the atmosphere, and precluding the formation of a surface semi-solid "skin." Thus, the modified process can produce KET-loaded CA nanofibers with smaller diameters, more uniform structures, and smoother surfaces. It avoids fiber surface collapse, and prevents surface wrinkles forming on the fibers. Single fluid electrospinning can do none of these things, and hence fiber F2 has more desirable properties than F1.

However, when an excessive sheath flow rate was used, such as in the case of F3 (see Fig. 2i), the surrounding solvent remained with the core fluid for a prolonged period of time and would have broken up into separate segments along the core jet due to its lack of viscoelasticity (Fig. 6c). It is postulated that this divided sheath solvent might mix with the core fluid locally to form sections of the fluid jet with different polymer concentrations, resulting in nanofibers with mixed morphologies (lines, spindrils, and clumps). Even so, the F3 fibers all showed smooth surfaces, in contrast to F4 which contained flat beads full of wrinkles (Fig. 2h).

4. Conclusions

A modified coaxial electrospinning process using only a solvent mixture as sheath fluid was successfully developed for the preparation of KET-loaded CA nanofibers. With a suitable sheath-to-core flow rate ratio, nanofibers prepared from the coaxial process had a smaller average diameter, narrower size distribution (240 ± 30 nm), more uniform structures and smoother surface morphologies than those generated *via* single fluid electrospinning (which had diameters of 680 ± 150 nm). While the single fluid process did result in KET dispersed in an amorphous state in CA-based fibers, with the fibers providing a sustained drug release profiles over 144 h *via* a Fickian diffusion mechanism, the fibers from the modified process offered a better zero-order drug release profile with a smaller tailing residue.

The influence of sheath solvents on the formation of nanofibers has been considered. The retardation of core solvent evaporation is believed to be the key reason underlying the preparation of thinner fibers in the modified coaxial process. This retains the core jet in a fluid state for longer, allowing it to be subjected to electrical drawing for an extended period of time. The sheath solvents may also act as a bridge for the mass transfer of solvent from the core fluids to the atmosphere, facilitating gradual core jet solidification. It is clear that the modified coaxial electrospinning process reported herein extends the capability of electrospinning to fabricate functional polymer nanofibers with enhanced quality.

Acknowledgments

This work was supported by the scientific starting funds for young teachers of the University of Shanghai for Science and Technology (No. 10-00-310-001), Grant 10JC1411700 from the Science and Technology Commission of Shanghai Municipality, and the National Science Foundation of China (No. 51173107).

References

Abou-Zeid, N. Y., Waly, A. I., Kandile, N. G., Rushdy, A. A., El-Sheikh, M. A., & Ibrahim, H. M. (2011). Preparation, characterization and antibacterial properties of cyanoethylchitosan/cellulose acetate polymer blended films. *Carbohydrate Polymers*, *84*(1), 223–230.

Ahn, Y., Hu, D. H., Hong, J. H., Lee, S. H., Kim, H. J., & Kim, H. (2012). Effect of co-solvent on the spinnability and properties of electrospun cellulose nanofiber. *Carbohydrate Polymers*, *89*(2), 340–345. http://dx.doi.org/10.1016/j.carbpol.2012.03.006

Anitha, S., Brabu, B., Thiruvadigal, D. J., Gopalakrishnan, C., & Natarajan, T. S. (2012). Optical, bactericidal and water repellent properties of electrospun nanocomposite membranes of cellulose acetate and ZnO. *Carbohydrate Polymers*, *87*(2), 1065–1072.

Deng, H., Li, X., Ding, B., Du, Y., Li, G., Yang, J., et al. (2011). Fabrication of polymer/layered silicate intercalated nanofibrous mats and their bacterial inhibition activity. *Carbohydrate Polymers*, *83*(2), 973–978.

Deng, H., Zhou, X., Wang, X., Zhang, C., Ding, B., Zhang, Q., et al. (2010). Layer-by-layer structured polysaccharides film-coated cellulose nanofibrous mats for cell culture. *Carbohydrate Polymers*, *80*(2), 474–479.

Díaz, J. E., Barrero, A., Márquez, M., & Loscertales, I. G. (2006). Controlled encapsulation of hydrophobic liquids in hydrophilic polymer nanofibers by co-electrospinning. *Advanced Functional Materials*, *16*(16), 2110–2116.

Fridrikh, S. V., Yu, J. H., Brenner, M. P., & Rutledge, G. C. (2003). Controlling the fiber diameter during electrospinning. *Physical Review Letters*, *90*(14), 144502.

Greiner, A., & Wendorff, J. H. (2007). Electrospinning: A fascinating method for the preparation of ultrathin fibers. *Angewandte Chemie International Edition*, *46*(30), 5670–5703.

Han, D., & Gouma, P. I. (2006). Electrospun bioscaffolds that mimic the topology of extracellular matrix. *Nanomedicine: Nanotechnology, Biology and Medicine*, *2*(1), 37–41.

Huang, Z. M., Zhang, Y. Z., Kotaki, M., & Ramakrishna, S. (2003). A review on polymer nanofibers by electrospinning and their applications in nanocomposites. *Composites Science and Technology*, *63*(15), 2223–2253.

Kanjanapongkul, K., Wongsasulak, S., & Yoovidhya, T. (2010a). Prediction of clogging time during electrospinning of zein solution: Scaling analysis and experimental verification. *Chemical Engineering Science*, *65*(18), 5217–5225.

Kanjanapongkul, K., Wongsasulak, S., & Yoovidhya, T. (2010b). Investigation and prevention of clogging during electrospinning of zein solution. *Journal of Applied Polymer Science*, *118*(3), 1821–1829.

Khatri, Z., Wei, K., Kim, B. S., & Kim, I. S. (2012). Effect of deacetylation on wicking behavior of co-electrospun cellulose acetate/polyvinyl alcohol nanofibers blend. *Carbohydrate Polymers*, *87*(3), 2183–2188.

Kim, C. J. (1995). Compressed doughnut-shaped tablets with zero-order release kinetics. *Pharmaceutical Researches*, *12*(7), 1045–1048.

Ma, G., Fang, D., Liu, Y., Zhu, X., & Nie, J. (2012). Electrospun sodium alginate/poly(ethylene oxide) core–shell nanofibers scaffolds potential for tissue engineering applications? *Carbohydrate Polymers*, *87*(1), 737–743.

Ma, Z., Kotaki, M., & Ramakrishna, S. (2005). Electrospun cellulose nanofiber as affinity membrane. *Journal of Membrane Science*, *265*(1–2), 115–123.

Moghe, A. K., & Gupta, B. S. (2008). Co-axial electrospinning for nanofiber structures: Preparation and applications. *Polymer Reviews*, *48*(2), 353–377.

Peppas, N. A. (1985). Analysis of Fickian and non-Fickian drug release from polymers. *Pharmaceutica Acta Helvetiae*, *60*(4), 110–111.

Qi, H., Sui, X., Yuan, J., Wei, Y., & Zhang, L. (2010). Electrospinning of cellulose-based fibers from NaOH/urea aqueous system. *Macromolecular Materials and Engineering*, *295*(8), 695–700.

Son, W. K., Youk, J. H., Lee, T. S., & Park, W. H. (2004). Electrospinning of ultrafine cellulose acetate fibers: Studies of a new solvent system and deacetylation of ultrafine cellulose acetate fibers. *Journal of Polymer Science Part B: Polymer Physics*, *42*(1), 5–11.

Taepaiboon, P., Rungsardthong, U., & Supaphol, P. (2007). Vitamin-loaded electrospun cellulose acetate nanofiber mats as transdermal and dermal therapeutic agents for vitamin A acid and vitamin E. *European Journal of Pharmaceutics and Biopharmaceutics*, *67*(2), 387–397.

Tian, Y., Wu, M., Liu, R., Li, Y., Wang, D., Tan, J., et al. (2011). Electrospun membrane of cellulose acetate for heavy metal ion adsorption in water treatment. *Carbohydrate Polymers*, *83*(2), 743–748.

Tsioptsias, C., Sakellariou, K. G., Tsivintzelis, I., Papadopoulou, L., & Panayiotou, C. (2010). Preparation and characterization of cellulose acetate–Fe_2O_3 composite nanofibrous materials. *Carbohydrate Polymers*, *81*(4), 925–930.

Tungprapa, S., Jangchud, I., & Supaphol, P. (2007). Release characteristics of four model drugs from drug-loaded electrospun cellulose acetate fiber mats. *Polymer*, *48*(17), 5030–5041.

Tungprapa, S., Puangparn, T., Weerasombut, M., Jangchud, I., Fakum, P., Semongkhol, S., et al. (2007). Electrospun cellulose acetate fibers: Effect of solvent system on morphology and fiber diameter. *Cellulose*, *14*(6), 563–575.

Wongsasulak, S., Patapeejumruswong, M., Weiss, J., Supaphol, P., & Yoovidhya, T. (2010). *Journal of Food Engineering*, *98*(3), 370–376.

Wu, X. M., Branford-White, C., Zhu, L. M., Chatterton, N. P., & Yu, D. G. (2010). Ester prodrug-loaded electrospun cellulose acetate fiber mats as transdermal drug delivery systems. *Journal of Materials Science: Materials in Medicine*, *21*(8), 2403–2411.

Yang, J. M., & Yu, D. G. (2012). Co-axial electrospinning with sodium thiocyanate solution for preparing polyacrylonitrile nanofibers. *Journal of Polymer Research*, *19*(2), 9789.

Yarin, A. L. (2011). Coaxial electrospinning and emulsion electrospinning of core–shell fibers. *Polymers Advanced Technologies*, *22*(3), 310–317.

Yeo, L. Y., & Friend, J. R. (2006). Electrospinning carbon nanotube polymer composite nanofibers. *Journal of Experimental Nanoscience*, *1*(2), 177–209.

Yu, D. G., Branford-White, C., Bligh, S. W. A., White, K., Chatterton, N. P., & Zhu, L. M. (2011). Improving polymer nanofiber quality using a modified co-axial electrospinning process. *Macromolecular Rapid Communications*, *32*(9–10), 744–750.

Yu, D. G., Branford-White, C., Chatterton, N. P., White, K., Zhu, L. M., Shen, X. X., et al. (2010). Electrospinning of concentrated polymer solutions. *Macromolecules*, *43*(24), 10743–10746.

Yu, D. G., Lu, P., Branford-White, C., Yang, J. H., & Wang, X. (2012). Polyacrylonitrile nanofibers prepared using co-axial electrospinning with LiCl solution as sheath fluid. *Nanotechnology*, *22*(43), 435301.

Yu, D. G., Shen, X. X., Branford-white, C., White, K., Bligh, S. W. A., & Zhu, L. M. (2009). Oral fast-dissolving drug delivery membranes prepared from electrospun polyvinylpyrrolidone ultrafine fibers. *Nanotechnology*, *20*(5), 055104.

Yu, D. G., Williams, G. R., Gao, L. D., Bligh, S. W. A., Yang, J. H., & Wang, X. (2012). Coaxial electrospinning with sodium dodecylbenzene sulfonate solution for high quality polyacrylonitrile nanofibers. *Colloids and Surface Part A: Physicochemical and Engineering Aspects*, *396*(2), 161–168.

Yu, D. G., Zhu, L. M., Branford-White, C., Bligh, S. W. A., & White, K. (2011). Coaxial electrospinning with organic solvent for controlling the size of self-assembled nanoparticles. *Chemical Communications*, *47*(4), 1216–1218.

Yu, J. H., Fridrikh, S. V., & Rutledge, G. C. (2004). Production of submicrometer diameter fibers by two-fluid electrospinning. *Advanced Materials*, *16*(17), 1562–1566.

Zenis, Y. (2004). Spinning continuous fibers for nanotechnology. *Science*, *304*(5679), 1917–1919.

Zhang, J. F., Yang, D. Z., Xu, F., Zhang, Z. P., Yin, R. X., & Nie, J. (2009). Electrospun core–shell structure nanofibers from homogeneous solution of poly(ethylene oxide)/chitosan. *Macromolecules*, *42*(14), 5278–5284.